Supporting Information

Spectral Management in Upconverting Sesquioxide through Matrix Doping

Dekang Xu,[a] Hao Lin,[a] Anming Li,[a] Shenghong Yang,[a] Yueli Zhang*[a,b]

[a]School of Physics and Engineering, Sun Yat-sen University, Guangzhou 510275, PR China

[b]State Key Laboratory of Crystal Material, Shandong University, Jinan 250100, PR China

*Corresponding author: stszyl@mail.sysu.edu.cn

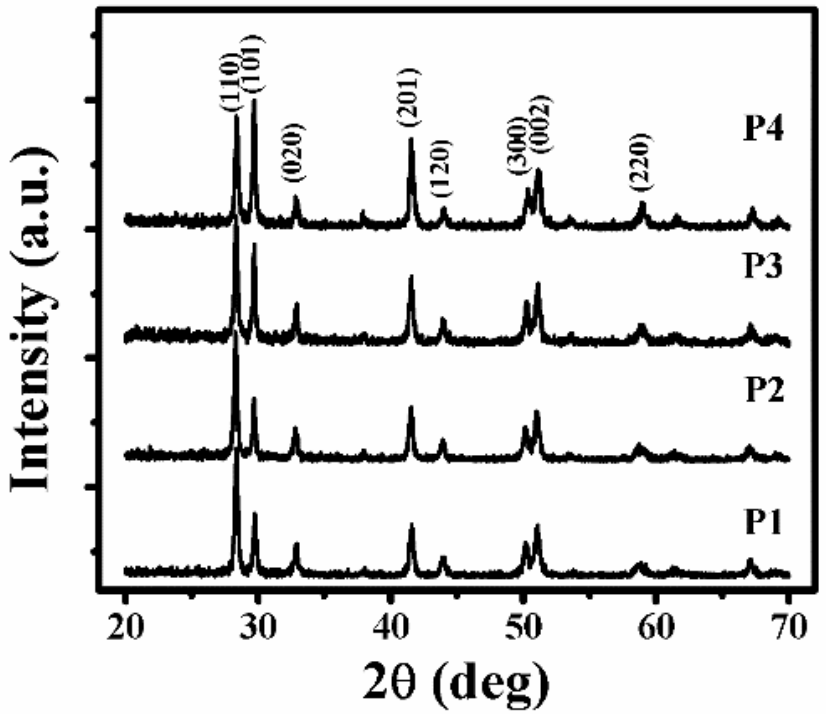

Fig. S1 XRD patterns of all codoped precursors, showing typical hexagonal structures. One can also observe that the relative intensity of (110) and (101) orientation is increasing along with samples with augmented NaOH content, indicating the growth orientation of precursors may vary with different NaOH content. According to the results dealt with heat treatment, the F-related compound appears as in the form of GdOF. The precursors do not show any signs of F-related compound due to the similar structures of hexagonal $Gd(OH)_3$ and hexagonal $Gd(OH)_{3-x}F_x$ according to the previous reports [(a) J. L. Zhuang, X. F. Yang, J. X. Fu, C. L. Liang, M. M. Wu, J. Wang and Q. Su, *Cryst. Growth Des.*, 2013, **13**, 2292-2297; (b) B. Q. Shao, Q. Zhao, W. Z. Lv, M. M. Jiao, W. Lv and H. P. You, *J. Mater. Chem. C*, 2015, **3**, 1091-1098]. As the F^-/OH^- ratio increases, partial $Gd(OH)_3$ turns into $Gd(OH)_{3-x}F_x$ due to the ion exchange of OH^- with F^-, which leads to the unchangeable structures.

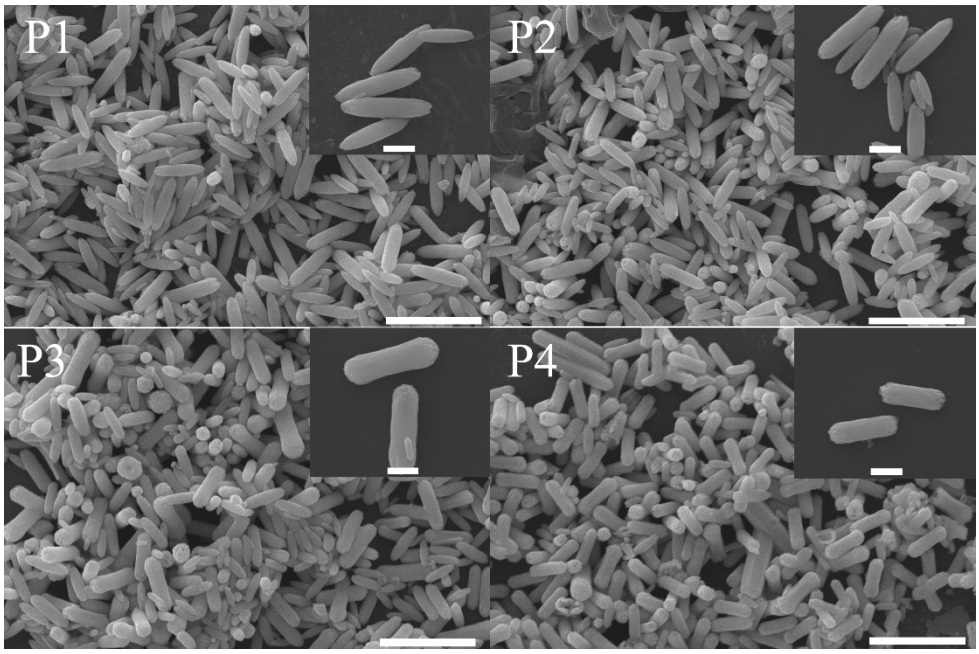

Fig. S2 SEM images of all precursors. (Scale bar = 5 μm) Insets show the magnified morphologies of all precursors. (Scale bar = 1 μm) One can also observe that both ends of rod-like crystals are sharp with high NaOH content, and gradually become blunter with decreasing NaOH content, indicating the orientation growth of the microcrystals. As can be seen from Fig. S1, while the ratio of (110) and (101) decreases along with lower NaOH content, both ends of rod-like become blunter, revealing that the axis along the rod is (110) orientation.

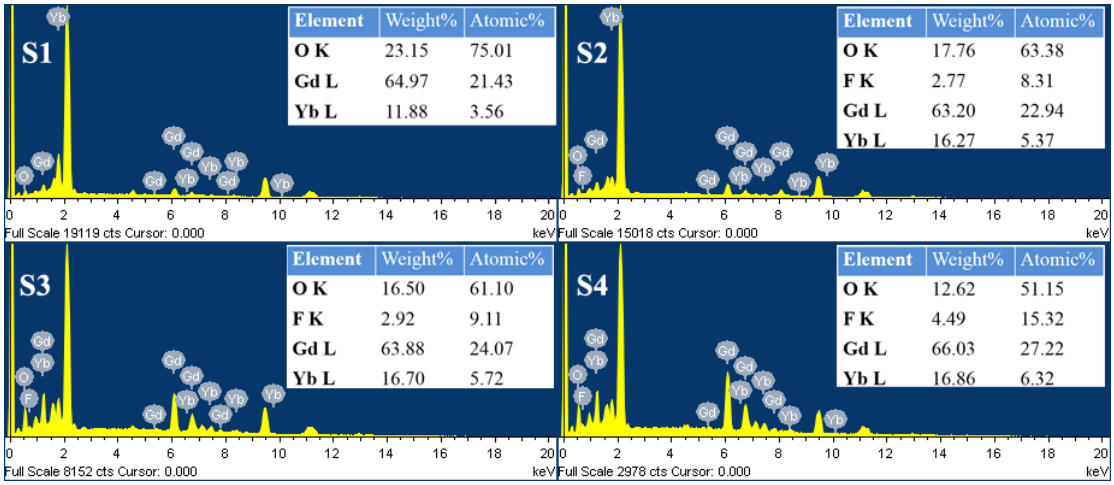

Fig. S3 EDX spectra of all calcined samples. The element analysis shows only Gd, O, and Yb elements, and the lanthanide ions of all samples are almost unchanged (Er^{3+} is ignored due to minor doping), which can be seen from elemental weight results: total lanthanide ions weight ratio ($Gd_{weight}\%$ + $Yb_{weight}\%$) is 76.85% for S1, 79.47% for S2, 80.58% for S3, and 82.89% for S4, respectively. Moreover, one can find out that the content of fluorine ions becomes larger from S1 to S4. Due to the incorporation of GdOF, oxygen content hence reduces, as can be seen from the decreasing weight and atomic ratio of oxygen ions (75.01 at% for S1, 63.38 at% for S2, 61.10 at% for S3, and 51.15 at% for S4).

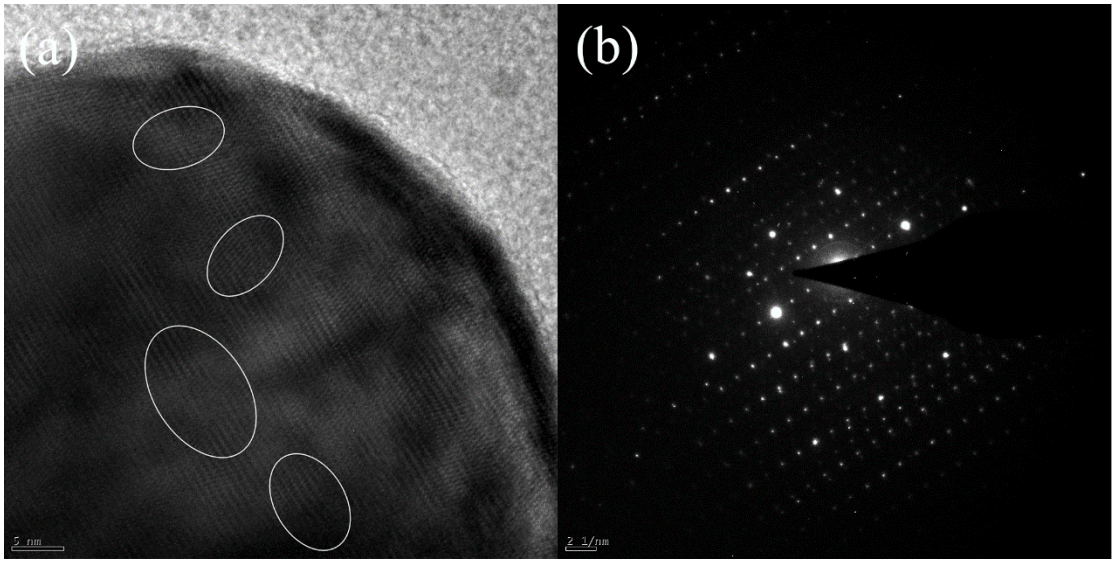

Fig. S4 High-resolution TEM (HRTEM) image (a) and the corresponding selected area electron diffraction (SAED) pattern (b) of S4. From the HRTEM image, some lattice distortions can be observed (as shown in the two lower elliptical regions for example). One can also find out some different lattice fringes, with various orientations, appear in the same particle (as shown in the two upper elliptical regions for example). Moreover, according to the SAED pattern, two sets of crystal lattices can be seen obviously. If one looks carefully, there are always pairs of diffraction spots closed to each other, which is due to the slightly difference of lattice distances between Gd_2O_3 and GdOF. The above results conclude that our product is not single-crystalline, and further verify the fact that the GdOF structure is homogeneously doped into Gd_2O_3 matrix.

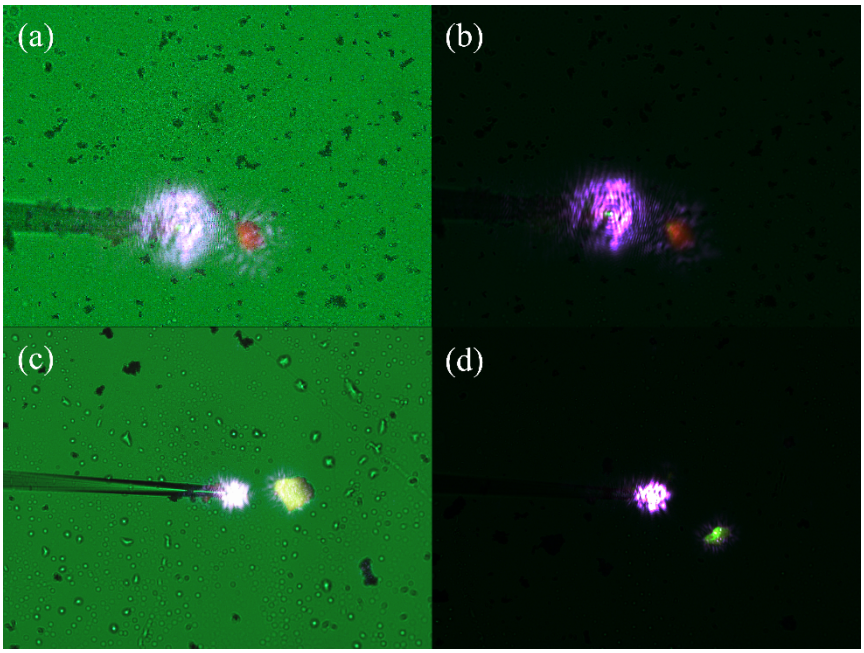

Fig. S5 Optical microscopy images of sample S1 (a,b) and S4 (c,d) for their bright (a,c) and dark (b,d) field fluorescence near the tip of a laser optical fiber that emits 980 nm light. Note that the violet scattering light is produced due to second harmonic generation within the laser fiber.

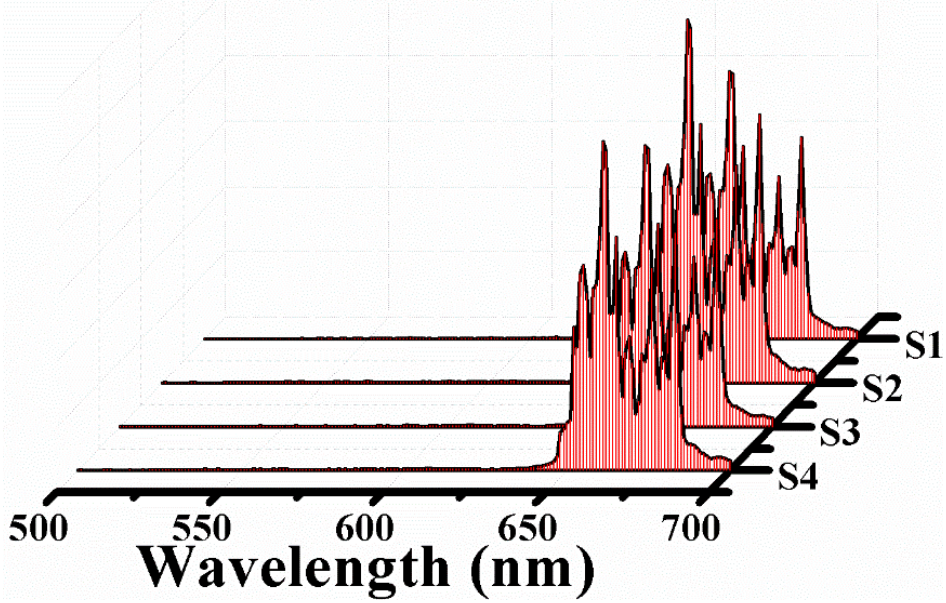

Fig. S6 UC emission spectra of samples without adding NaF, showing the only red emission bands and comparable luminescence intensities of all samples.

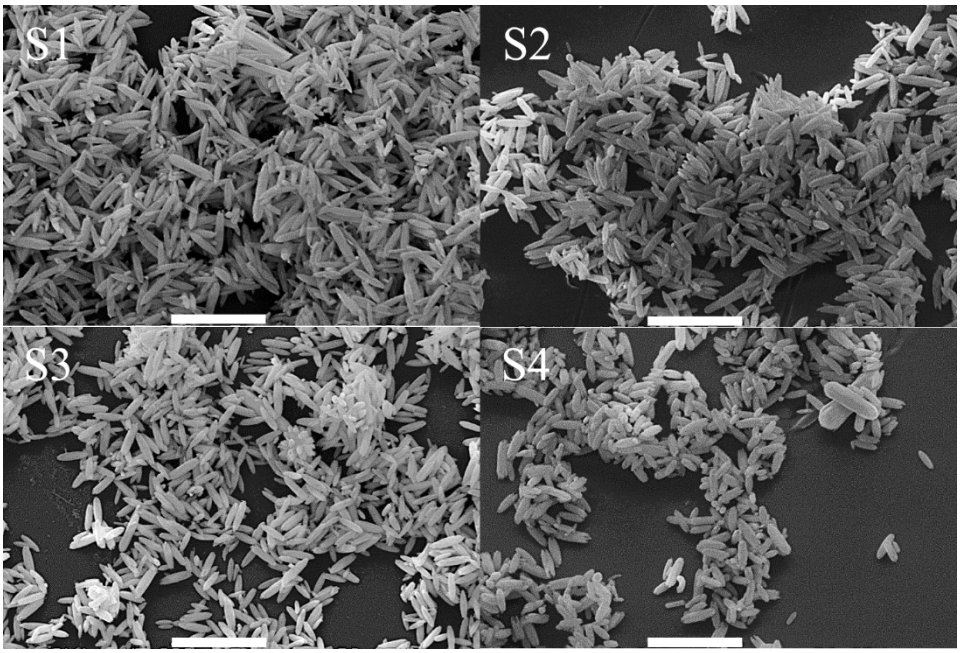

Fig. S7 SEM images of all samples without adding NaF, showing the similar morphologies of their counterparts with NaF and demonstrating the fact that the spectral tuning is not relevant to the particle morphology. (Scale bar = 5 μm)

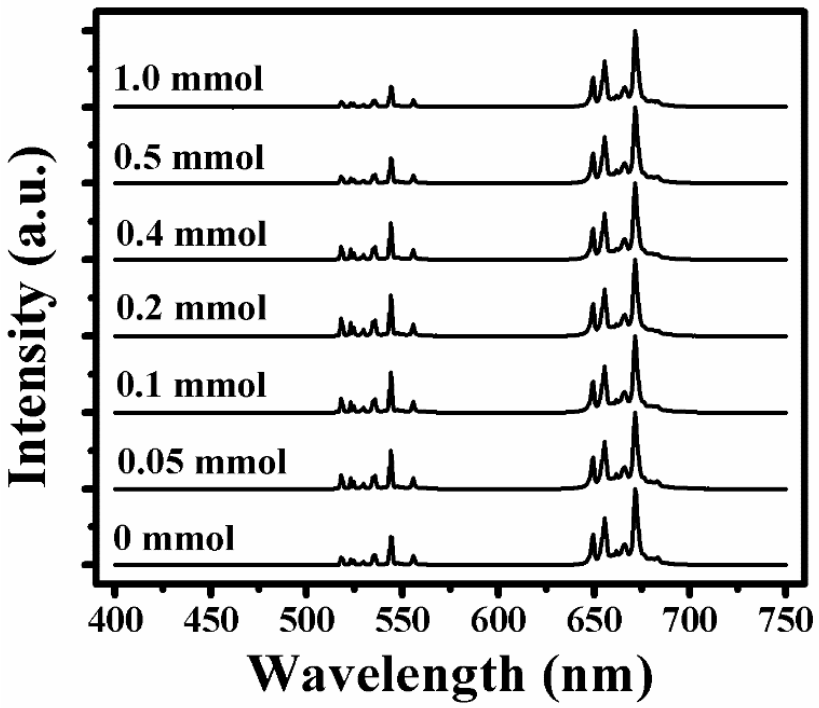

Fig. S8 UC emission spectra of samples derived with different EDTA, showing almost invariable relative intensity of red emission to green emission.

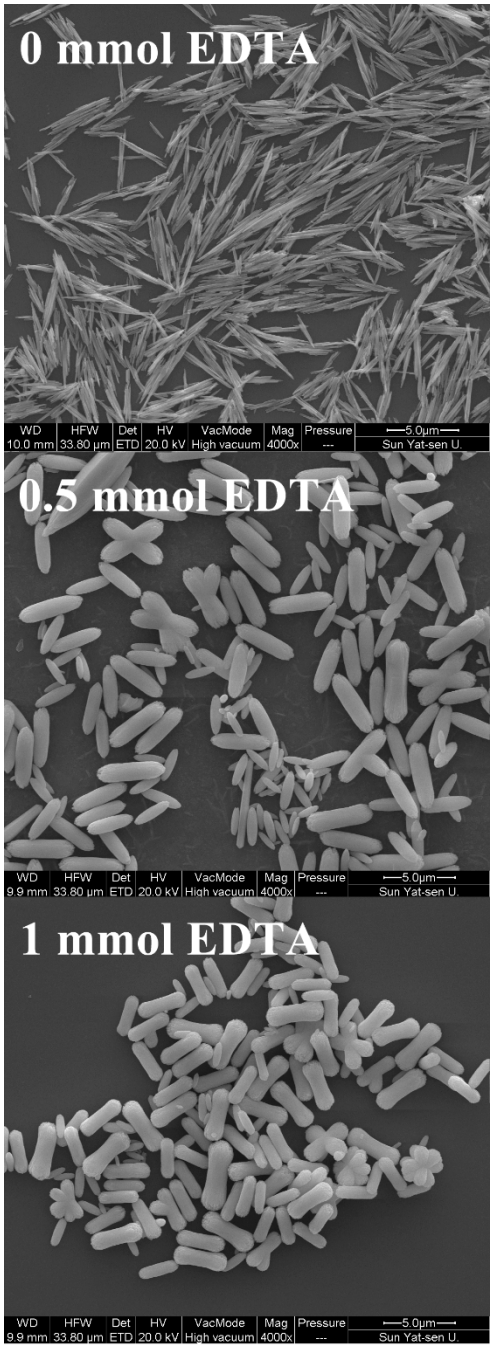

Fig. S9 SEM images of precursors with different amount of EDTA. Precursor without EDTA additive show nanosized rod-like particles. With increasing amount of EDTA, the particles become much fatter, owing to the coupling interaction of EDTA to bind the nanosized rod-like particles together. Nevertheless, the varying morphologies do not influence the emission behavior of all samples.

Discussion on Energy Transfer Mechanisms for Sample S1 and S4

A set of coupled differential equations is used to describe the instantaneous populations and energy transfer between Er^{3+}-Yb^{3+} based on the proposed energy transfer models shown in Fig. 6 (e).

$$\frac{dN_i}{dt} = \sum_{ij,kl}\left(\omega_{ji,lk}^{ET} N_j N_l - \omega_{ij,kl}^{ET} N_i N_k\right) + \left(\omega_{i+1,i}^{NR} N_{i+1} - \omega_{i,i-1}^{NR} N_i\right) - A_i N_i$$

Generally, the population density of Yb^{3+} can be described as follows:

$$\frac{dN_{Yb1}}{dt} = \sigma\rho N_{Yb0} - \sum_i \omega_i N_i N_{Yb1} - A_{Yb1} N_{Yb1}$$

which then deduces that: $N_{Yb1} \sim \rho$. In the following equations, N_1, N_2, N_3, N_4, N_{Yb0} and N_{Yb1} are the populations of the Er^{3+} $^4I_{13/2}$, $^4I_{11/2}$, $^4F_{9/2}$, $^2H_{11/2}/^4S_{3/2}$, Yb^{3+} $^2F_{7/2}$ and $^2F_{5/2}$ manifolds, respectively. ω_0, ω_1 and ω_2 are ET parameters between Yb^{3+} $^2F_{7/2} \rightarrow {}^2F_{5/2}$ and Er^{3+} $^4I_{15/2} \rightarrow {}^4I_{11/2}$, $^4I_{13/2} \rightarrow {}^4F_{9/2}$ and $^4I_{11/2} \rightarrow {}^4F_{7/2}$, respectively. ω_{21} and ω_{43} are MPR rates from Er^{3+} $^4I_{11/2} \rightarrow {}^4I_{13/2}$ and Er^{3+} $^2H_{11/2}/^4S_{3/2} \rightarrow {}^4F_{9/2}$, respectively. ω_b is the EBT rate to the Yb^{3+} ions. A_1, A_2, A_3 and A_4 are radiative rates of Er^{3+} $^4I_{13/2}$, $^4I_{11/2}$, $^4F_{9/2}$ and $^2H_{11/2}/^4S_{3/2}$ manifolds, respectively.

1) As to the model described for S1, the rate equations can be expressed as follows:

$$\begin{aligned}
\frac{dN_1}{dt} &= \omega_{21} N_2 + \omega_b N_4 N_{Yb0} - \omega_1 N_1 N_{Yb1} - A_1 N_1 \\
\frac{dN_2}{dt} &= \omega_0 N_0 N_{Yb1} - \omega_{21} N_2 - \omega_2 N_2 N_{Yb1} - A_2 N_2 \\
\frac{dN_3}{dt} &= \omega_1 N_1 N_{Yb1} + \omega_{43} N_4 - A_2 N_2 \\
\frac{dN_4}{dt} &= \omega_2 N_2 N_{Yb1} - \omega_{43} N_4 - \omega_b N_4 N_{Yb0} - A_4 N_4
\end{aligned}$$

Since the linear decay is the dominant depletion mechanism, the UC terms can be neglected, i.e., $\omega_1 N_{Yb1}$ and $\omega_2 N_{Yb1}$ can be ignored compared to $A_1 N_1$ and $A_2 N_2$, respectively. Solve the above equations, one can obtain:

$$\begin{aligned}
N_1 &\rightarrow a\rho^1 + b\rho^2 \\
N_2 &\rightarrow a\rho^1 \\
N_4 &\rightarrow a\rho^2 \\
N_3 &\rightarrow a\rho^2 + b\rho^3
\end{aligned}$$

which matches well with the slope values shown in Fig. 6 (a).

2) As to model for S4, the rate equations are as follows:

$$\frac{dN_1}{dt} = \omega_{21}N_2 + \omega_b N_4 N_{Yb0} - \omega_1 N_1 N_{Yb1} - A_1 N_1$$
$$\frac{dN_2}{dt} = \omega_0 N_0 N_{Yb1} - \omega_{21}N_2 - \omega_2 N_2 N_{Yb1} - A_2 N_2$$
$$\frac{dN_3}{dt} = \omega_1 N_1 N_{Yb1} + \omega_{43}N_4 - A_3 N_3$$
$$\frac{dN_4}{dt} = \omega_2 N_2 N_{Yb1} - \omega_b N_4 N_{Yb0} - \omega_{43}N_4 - A_4 N_4$$

In this sample, the ETU process becomes more and more important, so the linear decay terms such as A_1N_1 and A_2N_2 are comparable with $\omega_1 N_{\mathrm{Yb1}}$ and $\omega_2 N_{\mathrm{Yb1}}$. Consider the extreme condition when ETU process is the dominant depletion mechanism, one can get by solving the above equations:

$$N_1 \to a\rho^{-1} + b\rho^1$$
$$N_2 \to a\rho^0$$
$$N_3 \to a\rho^0 + b\rho^1$$
$$N_4 \to a\rho^1$$

Under such situation, both emissions (N_3 and N_4) exhibit linear relationship with excitation density. However, in fact, the ETU process is as important as LD process for the depletion of the intermediate manifolds due to the slight variation of the effective average Er^{3+}-Yb^{3+} distance as GdOF structure is doped into Gd_2O_3 host. Therefore, the real relationship between UC emissions and excitation density for S4 is the linear combination of Condition **1)** and **2)**, that is,

$$N_3 \to a\rho^1 + b\rho^2$$
$$N_4 \to a\rho^1 + b\rho^2$$

which coincides with the results as shown in Fig. 6 (b).